Lab on a Chip

PAPER

View Article Online
View Journal | View Issue

Cite this: *Lab Chip*, 2020, **20**, 3011

Organ-on-chip model shows that ATP release through connexin hemichannels drives spontaneous Ca^{2+} signaling in non-sensory cells of the greater epithelial ridge in the developing cochlea†‡

Flavia Mazzarda, [ab] Annunziata D'Elia, [ab] Roberto Massari, [a] Adele De Ninno, [c] Francesca Romana Bertani, [c] Luca Businaro, [c] Gaia Ziraldo, [ad] Veronica Zorzi, [ad] Chiara Nardin, [a] Chiara Peres, [a] Francesco Chiani, [a] Abraham Tettey-Matey, [a] Marcello Raspa, [a] Ferdinando Scavizzi, [a] Alessandro Soluri, [a] Anna Maria Salvatore, [a] Jun Yang [ef] and Fabio Mammano *[ag]

Prior work supports the hypothesis that ATP release through connexin hemichannels drives spontaneous Ca^{2+} signaling in non-sensory cells of the greater epithelial ridge (GER) in the developing cochlea; however, direct proof is lacking. To address this issue, we plated cochlear organotypic cultures (COCs) and whole cell-based biosensors with nM ATP sensitivity (ATP-WCBs) at the bottom and top of an *ad hoc* designed transparent microfluidic chamber, respectively. By performing dual multiphoton Ca^{2+} imaging, we monitored the propagation of intercellular Ca^{2+} waves in the GER of COCs and ATP-dependent Ca^{2+} responses in overlying ATP-WCBs. Ca^{2+} signals in both COCs and ATP-WCBs were inhibited by supplementing the extracellular medium with ATP diphosphohydrolase (apyrase). Spontaneous Ca^{2+} signals were strongly depressed in the presence of *Gjb6*$^{-/-}$ COCs, in which connexin 30 (Cx30) is absent and connexin 26 (Cx26) is strongly downregulated. In contrast, spontaneous Ca^{2+} signals were not affected by replacement of *Panx1*$^{-/-}$ with *Panx1*$^{+/+}$ COCs in the microfluidic chamber. Similar results were obtained by estimating ATP release from COCs using a classical luciferin–luciferase bioluminescence assay. Therefore, connexin hemichannels and not pannexin 1 channels mediate the release of ATP that is responsible for Ca^{2+} wave propagation in the developing mouse cochlea. The technological advances presented here have the potential to shed light on a plethora of unrelated open issues that involve paracrine signaling in physiology and pathology and cannot be addressed with standard methods.

Received 27th April 2020,
Accepted 2nd July 2020

DOI: 10.1039/d0lc00427h

rsc.li/loc

[a] *CNR Institute of Biochemistry and Cell Biology, Monterotondo, Rome, Italy. E-mail: fmazzarda@gmail.com, nunzia_delia@yahoo.it, roberto.massari@cnr.it, zira13@gmail.com, veronicazorzi.vimm@gmail.com, chiara.nardin@ibbc.cnr.it, chiara.peres@ibbc.cnr.it, francesco.chiani@cnr.it, abraham.matey@ibbc.cnr.it, marcello.raspa@cnr.it, ferdinando.scavizzi@cnr.it, alessandro.soluri@cnr.it, annamaria.salvatore@cnr.it*

[b] *Department of Science, Università degli Studi di Roma3, Rome, Italy*

[c] *CNR Institute for Photonics and Nanotechnology, Rome, Italy. E-mail: adele.deninno@ifn.cnr.it, francesca.bertani@cnr.it, luca.businaro@ifn.cnr.it*

[d] *Institute of Otorhinolaryngology, Università Cattolica del Sacro Cuore, Rome, Italy*

[e] *Department of Otorhinolaryngology Head and Neck Surgery, Xinhua Hospital, Shanghai Jiao Tong University School of Medicine, Shanghai, China. E-mail: dryangjunxinhua@163.com*

[f] *Shanghai Key Laboratory of Translational Medicine on Ear and Nose diseases, Shanghai, China*

[g] *Department of Physics and Astronomy "G. Galilei", University of Padova, Padua, Italy. E-mail: fabio.mammano@unipd.it*

† Data will be made available *via* University of Padova's Data Repository.

‡ Electronic supplementary information (ESI) available. See DOI: 10.1039/d0lc00427h

Introduction

Extracellular ATP modulates the function of both sensory and non-sensory cells in the inner ear (reviewed in ref. 1–3). In the developing cochlea, ATP triggers cytosolic Ca^{2+} concentration oscillations and propagation of intercellular Ca^{2+} waves that carry crucial biochemical information to the cochlear sensory epithelium.[4–6] The latter is subdivided into two embryologically distinct regions, the lesser epithelial ridge (LER) and the greater epithelial ridge (GER), which are separated by a pair of immature inner and outer pillar cells.[7–9] The GER encompasses the nascent inner sulcus, the tall columnar cells of the Kölliker organ,[10,11] the inner hair cells (IHCs) and their abutting supporting cells.[12,13] Ca^{2+} waves arise spontaneously in the GER[14–19] and appear to play a crucial role in normal development of the cochlear sensory epithelium, hearing acquisition, functional maturation of hair

cells,[20–23] redox homeostasis and age-related hearing loss.[24] A wealth of experimental data and modeling studies support the notion that Ca^{2+} wave propagation in the developing cochlea is sustained by the release of ATP from the cytosol of non-sensory cells to the endolymph,[18,25–27] in which baseline ATP concentration ([ATP]) is in the low nM range.[28,29] Genetic interference experiments support a crucial role for Cx26 and Cx30, the two major cochlear connexins,[30–32] in intercellular Ca^{2+} wave propagation in the developing cochlea[17,18,25,33–36] (reviewed in ref. 2 and 37). However, direct proof that ATP release through connexin hemichannels drives spontaneous Ca^{2+} wave propagation in the GER is lacking.

To address this critical issue, we used two global knock out (KO) mouse strains, namely connexin 30 KO (*Gjb6*$^{-/-}$; MGI: 2447863) and pannexin 1 KO (*Panx1*$^{-/-}$; MGI: 5310802). *Gjb6*$^{-/-}$ mice fail to acquire hearing and do not develop endocochlear potential.[17,38] Furthermore, they show defects of the endothelial barrier in capillaries of the *stria vascularis*[39] and impaired gap junction-mediated transfer of the fluorescent D-glucose derivative 2-NBDG.[40] Accordingly, not only is Cx30 not expressed, but also Cx26 levels are severely reduced in the developing cochlea of this KO strain.[33] In contrast, *Panx1*$^{-/-}$ mice[25,41] have an increased susceptibility for atrial fibrillation and show a QT-prolongation cardiac phenotype.[42] However, their hearing sensitivity, outer hair cell-based "cochlear amplifier" and cochlear nerve function, analyzed by auditory brainstem response (ABR) and distortion product otoacoustic emission (DPOAE) recordings, are normal, together with connexin expression and gap-junction coupling in the developing organ of Corti.[34]

As detailed below, we developed an innovative organ-on-chip model which, by the coupling of microfluidic technology, whole cell-based biosensors (WCBs)[43] with nM sensitivity to extracellular ATP[25] and multiphoton imaging, allowed systematic addressing of purinergic signaling in COCs obtained from the above mentioned KO mice. Our results provide direct evidence that ATP release through connexin hemichannels drives spontaneous Ca^{2+} wave propagation in the GER.

Methods

Animals

All animals (*Mus musculus*) used in this study (see Table 1) were bred at the National Research Council-Institute of Biochemistry and Cell Biology (CNR-IBBC), Infrafrontier/ESFRI-European Mouse Mutant Archive (EMMA), Specific Pathogen-Free (SPF) barrier unit (Monterotondo Scalo, Rome, Italy). Mice were housed in individually ventilated caging systems (Tecniplast, Gazzada, Italy) at a temperature (*T*) of 21 ± 2 °C, relative humidity (RH) of 55 ± 15% with 50–70 air changes per hour (ACH) and under controlled (12 : 12 hour) light–dark cycles (7 am–7 pm). Mice had *ad libitum* access to water and a standard rodent diet (Emma 23, Mucedola, Settimo Milanese, Italy). Both male and female homozygous *Gjb6*$^{-/-}$ [EMMA ID (EM): 00323] or *Panx1*$^{-/-}$ (EM: 11476) pups at post-natal day 5 (P5) and their wild type P5 siblings (*Gjb6*$^{+/+}$, *Panx1*$^{+/+}$) were used. The background strains of these mice were C57BL/6J for *Gjb6*$^{-/-}$ and C57BL/6N for *Panx1*$^{-/-}$ mice. Note that there is no discernible difference in the auditory phenotype of the closely related C57BL/6J and C57BL/6N mouse strains.[44]

Experimental animals were culled by trained personnel using gaseous anaesthesia followed by a rising concentration of CO_2. All the experimental procedures were agreed upon, reviewed and approved by local animal welfare oversight bodies and were performed with the approval and direct supervision of the CNR-IBBC/Infrafrontier—Animal Welfare and Ethical Review Body (AWERB), in accordance with general guidelines regarding animal experimentation, approved by the Italian Ministry of Health, in compliance with the Legislative Decree 26/2014 (ref. Project licence no. 68/2016-PR), transposing the 2010/63/EU Directive on protection of animals used in research. This work was also conducted based on recommendations from both ARRIVE and PREPARE guidelines.[45,46]

Table 1 List of all mice used for this study

Genotype	*Gjb6*$^{+/+}$	*Gjb6*$^{-/-}$	*Panx1*$^{+/+}$	*Panx*$^{-/-}$	C57BL6/N
Male	*5*	*5*	*7*	7	2
Female	*5*	*5*	*6*	6	1
Total	*10*	*10*	*13*	13	3

Genotyping

Panx1 mice were genotyped according to published protocols by standard PCR on extracted mouse tail tips using the following primers:

Panx1 f: 5′-GGAAAGTCAACAGAGGTACCC-3′.

Panx1 r: 5′-CTTGGCCACGGAGTATGTGTT-3′.

LacZ: 5′-GTCCCTCTCACCACTTTTCTTACC-3′.

Mice with normal *Panx1* alleles (*Panx1*$^{+/+}$) were targeted by the above f and r primers and identified by a 330 bp band, whereas *Panx1*$^{-/-}$ were targeted by primers *Panx1* f and LacZ, and were identified by a 630 bp band. *Panx1*$^{\pm}$ mice were identified by the simultaneous presence of a 330 bp and a 630 bp band. Primer pairs for *Gjb6*$^{-/-}$ mice were specific for the wild type alleles:

Gjb6 f: 5′-GGTACCTTCTACTAATTAGCTTGG-3′,

Gjb6 r: 5′-AGGTGGTACCCATTGTAGAGGAAG-3′.

To visualize the deletion, primers specific for the *lacZ* region (that flanks the deleted allele) were used in combination with the corresponding wild type forward primer:

*Gjb6*lac 5′-AGCGAGTAACAACCCGTCGGATTC-3′.

Mice with normal *Gjb6* alleles (*Gjb6*$^{+/+}$) were identified by a 544 bp band, whereas *Gjb6*$^{-/-}$ mice were identified by a 460 bp band. See also Table 1.

Study design

In order to construct the optimal experimental design and estimate the minimum number of animals necessary for the experiments (sample size of the groups), for each type of

experiment and for each genetically modified and control strain ($Gjb6^{-/-}$, $Gjb6^{+/+}$, $Panx1^{-/-}$, $Panx1^{+/+}$), we set probability $\alpha = 5\% = 0.05$ for the type I error in the t test. Then, fixing $\beta = 4\alpha = 20\% = 0.2$ to obtain a test power of $1 - \beta = 80\% = 0.8$, we computed the number n of each of the two samples to be compared using the formula:[47]

$$n > 2\left[\frac{(z_{\alpha/2} + z_{\beta})\cdot\sigma}{\Delta}\right]^2$$

with $z_{\alpha/2} = 1.96$ and $z_{\beta} = 0.842$. Based on experiments of the same type carried out in prior work, we quantified the variability of the data (variance, σ^2) and established the minimum difference $\Delta = \mu_1 - \mu_2$ between averages that had a biological significance. By expressing both parameters as percentages and setting $\sigma = 12.5\% = 0.125$ and $\Delta = 16\% = 0.16$, we obtained $n > 9.58$. The actual number of mice is provided in Table 1. To minimize subjective bias, sample identity (*e.g.* genotypes) was randomized by associating an identification number to each sample before processing. No sample was excluded from the analysis.

Preparation of COCs

P5 mouse pups were humanely euthanized, both cochleae were carefully removed, quickly dissected in ice-cold HEPES buffered (pH 7.2) HBSS (Cat. No. 14025050, Thermo Fisher Scientific, Waltham, MA, USA) and placed onto 5 mm round glass coverslips coated with Cell-Tak (Cat. No. 354240, Corning, Corning, NY, USA). COCs were incubated overnight in DMEM/F12 (Cat. No. 11320-074, Thermo Fisher Scientific) supplemented with 5% FBS (Cat. No. 10270-106, Thermo Fisher Scientific) and 100 μg ml^{-1} ampicillin (Cat. No. A0166, Merck, St. Louis, MO, USA) at 37 °C in a humid air atmosphere enriched with 5% CO_2. The tectorial membrane was carefully removed prior to each experiment.

Generation and culture of ATP-WCBs

To generate ATP-WCBs, we transduced HEK293-T cells (CRL-3216™, ATCC, Manassas, VI, USA) with a lentiviral vector encoding P2Y purinoceptor 2 ($P2Y_2R$), a high affinity G-protein coupled receptor that mobilizes Ca^{2+} from intracellular stores upon binding extracellular ATP.[48,49] By using the Gibson assembly technique,[50] we inserted the $P2Y_2R$ complementary DNA (a gift of Marta Fumagalli, Laboratory of Molecular and Cellular Pharmacology of Purinergic Transmission, University of Milan) into a 3rd generation backbone vector (pUltra-hot, Addgene plasmid #24130, Addgene, Watertown, MA, USA; a gift from Malcolm Moore) that uses 2A self-cleaving peptide technology[51] to express the protein of interest ($P2Y_2R$) and the mCherry fluorescent reporter[52] in a 1 : 1 ratio under the UbC promoter. Viral particles based on this transfer vector were produced using a standard protocol;[53] thereafter the virus-containing supernatant was harvested and stored into cryovials in 1 ml aliquots at −80 °C.

Prior to viral transduction, parental HEK293-T cells were maintained in DMEM/F12 (Cat. No. 11320-074, Thermo Fisher Scientific) containing 10% heat inactivated FBS (Cat. No. 10270-106, Thermo Fisher Scientific), 1% penicillin/streptomycin (Cat. No. 15070063, Merck), 1% L-glutamine (Cat. No. 25030024, Merck) and 1% sodium pyruvate (Cat. No. 11360070, Merck). Twenty-four hours before viral transduction (day 1), HEK293-T cells were trypsinized and plated onto 35 mm Petri dishes such that they would be 30–50% confluent at the time of transduction. On the day of transduction (day 2), the culture medium was removed and replaced with the thawed virus-containing supernatant. Sequa-brene (8 μg ml^{-1}, Cat. No. S2667, Merck; synonym: hexadimethrine bromide, polybrene) was added to each Petri dish, followed by gentle swirl to enhance transduction efficiency. HEK293-T cells were incubated overnight, at 37 °C under a controlled atmosphere of CO_2 (5%), in the virus-containing supernatant. The following day (day 3), the transduction medium was removed and replaced with 2 ml of complete culture medium. The percentage of HEK293-T transduced cells (>95%), henceforth referred to as WBCs, was estimated 48 hours post-transduction by fluorescence microscopy of the mCherry reporter.

Construction of the ATP dose–response curve for ATP-WCBs

ATP-WCBs were re-plated in black 96-well plates (Cat No. 655090, Greiner Bio-One Italia S.r.l, Cassina de Pecchi, Italy) and cultured for 24 hours as detailed above. Thereafter, ATP-WCBs were incubated for 2 hours at 37 °C and 5% CO_2 with the loading solution of the FLIPR Calcium 6 Assay Kit (Cat. No. R8190, Molecular Devices, San Jose, CA, USA). Ca^{2+}-Dependent fluorescence changes promoted by ATP binding to the $P2Y_2R$ were measured using a Varioskan LUX multimode microplate reader (Cat. No. VL0L00D0, Thermo Fisher Scientific) after injection of known amounts of ATP (from 0.1 nM to 1 μM) in the wells. To achieve the desired [ATP], a 1 mM stock solution was prepared by dissolving ATP (Cat. No. A1852, Merck) in PBS and diluting the stock in the loading solution of the FLIPR Calcium 6 Assay Kit.

Ca^{2+} imaging in individual ATP-WCBs

To visualize Ca^{2+} responses evoked by ATP in individual ATP-WCBs, the latter were plated on 12 mm ∅ coverslips and incubated for 30 min at 37 °C in serum-free DMEM (Cat. No. 10-017-CV, Corning, Corning, NY, USA) supplemented with the Ca^{2+}-selective fluorescent probe Fluo 8H™ AM (5 μM, dissociation constant K_d = 232 nM, Cat. No. 21091, AAT Bioquest, Sunnyvale, CA, USA). The incubation medium also contained Pluronic F-127 (0.1% w/v, Cat. No. P2443, Merck) and sulfinpyrazone (250 μM, Cat. No. S9509, Merck) to prevent dye sequestration and secretion.[54] To allow for de-esterification, coverslips with loaded ATP-WCBs were transferred to the stage of a custom-made spinning disk microscope[55] and perfused for 10 min at a flow rate of 0.1 mL min^{-1} with extracellular medium (EXM) containing (in mM): NaCl 135, KCl 5.8, $CaCl_2$ 1.3,

NaH_2PO_4 0.7, $MgCl_2$ 0.9, HEPES–NaOH 10, D-glucose 6, pyruvate 2, amino acids, and vitamins (pH 7.48, 307 mOsm). ATP dissolved in EXM was applied by pressure (5 pounds per square inch, PSI) using a PV820 pneumatic pico-pump (World Precision Instruments Inc., Sarasota, FL, USA) coupled to a glass microcapillary with an opening diameter of 4 μm placed under a 60× water immersion microscope objective (NIKON FLUOR, NA = 1.0, Nikon Corporation, Tokyo, Japan) near the center of the field of view and in close proximity to ATP-WCBs. For Ca^{2+} imaging, Fluo 8H™ fluorescence was excited using a 488 nm diode laser (Cat. No. COMPACT-150G-488-SM, World Star Tech, Markham, Ontario, Canada) by 45° reflection off a triband dichroic mirror (Cat. No. FF395/527/610-Di01, Semrock, Rochester, NY, USA). Fluo 8H™ fluorescence emission was filtered through a triband filter (Cat. No. FF425/527/685-25, Semrock) followed by a green band pass filter (Cat. No. ET535/30M, Chroma Technology Corp., Bellows Falls, VT, USA) located in front of a cooled s-CMOS camera (pco.edge, PCO AG, Kelheim, Germany) coupled to the microscope.[55] Suramin (150 μM; Cat. No. S2671, Merck) was used to reversibly inhibit the ATP-evoked Ca^{2+} responses (see Results).

Dual focal plane multiphoton Ca^{2+} imaging in COCs and ATP-WCBs

The day before the experiment, ATP-WCBs were plated on 12 mm ∅ coverslips at a density of 2×10^4 cells per cm^2. At experiment time, they were loaded with Fluo 8H™ AM as described above. COCs were plated on 5 mm ∅ coverslips the day before the experiment, and incubated for 45 min at 37 °C in serum-free DMEM supplemented with 20 μM Fluo 8H™ AM, Pluronic F-127 (0.1% w/v) and sulfinpyrazone (250 μM) at experiment time. To allow for de-esterification, both cultures were transferred into an *ad hoc* designed microfluidic chamber (Fig. 1), perfused for 10 min with EXM and placed on the stage of a custom-made two-photon microscope (Fig. 2) based on a Bergamo II architecture (Thorlabs Imaging System, Sterling, VI, USA). The polydimethylsiloxane (PDMS) insert of the chamber (Fig. 1b–d) included microfluidic channels connected by 25 mm stainless-steel tubing (AISI 316L, 0.25/0.12 mm, Unimed SA, CH-1007 Lausanne, Switzerland) and flexible external tubing (Tygon ST R-3603/R3607, Harvard Apparatus, Holliston, MA 01746 United States) to a proximally located peristaltic pump (P-70, Harvard Apparatus). This arrangement reduced the effective chamber volume to 10 μl and the total volume in the fluid path to 200 μl. The flow rate was kept ≤100 μl min^{-1} to minimize the effects of fluid shearing stress,[56] and perfusion was stopped during the image-recording session (which generally lasted 1 min). EXM (containing 2 mM Ca^{2+}) was replaced by LCS, a medium with an endolymph-like Ca^{2+} concentration (20 μM)[57] and an otherwise identical composition. LCS was supplemented either with the ATP analogue 6-*N*,*N*-diethyl-D-beta-gamma-dibromomethylene adenosine triphosphate (ARL67156, 100 μM, Cat. No. A265, Merck), or apyrase (40 U ml^{-1}, Cat. No. A6535, Merck), depending on the type of experiment (see Results).

The multiphoton system was equipped with two scanning heads, one with resonant-galvo (RG) mirrors and the other with galvo–galvo (GG) mirrors, and was coupled to a mode-

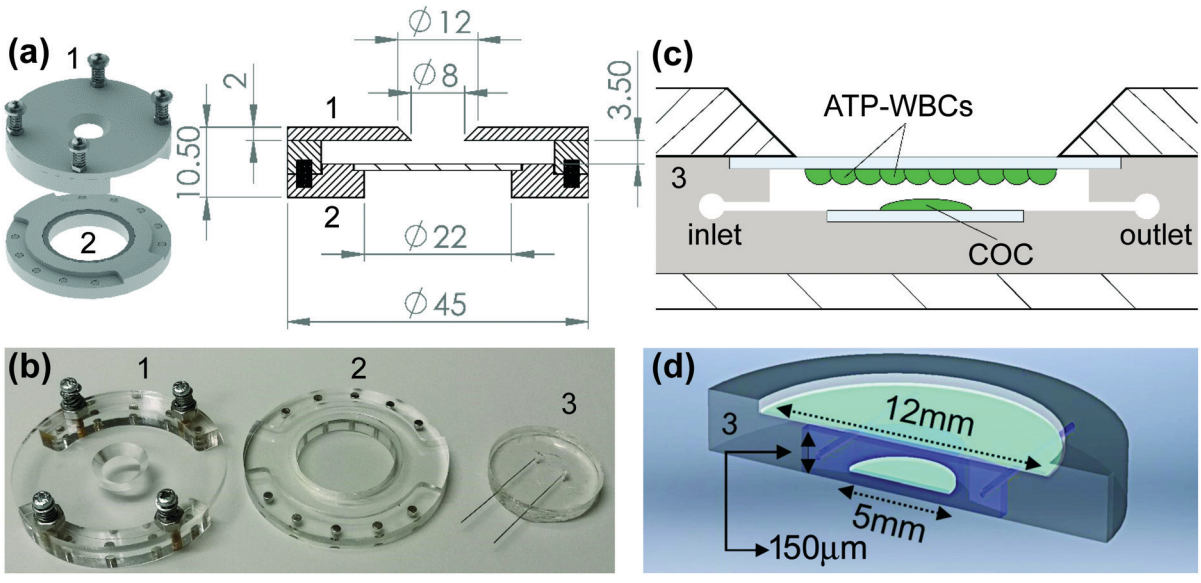

Fig. 1 Microfluidic chamber architecture. (a) 3D rendering and transverse section of plexiglass scaffold components (#1, top; #2, bottom) with dimensions in mm; a 25 mm ∅ Gorilla glass window seals off component #2. Note the array of magnets that hold the chamber together; the chamber is easily opened by misaligning the magnets with a twist. (b) Photograph of the disassembled chamber showing also the PDMS insert (#3); the four spring-loaded screws in #1 permit the spacing between components #1 and #2 to finely adapt to the thickness of insert #3. (c) Schematic drawing of component #3 carrying coverslips with cartoons of adherent ATP whole-cell biosensors (ATP-WCBs) at the top and cochlear organotypic culture (COC) at the bottom (not to scale). (d) 3D rendering of component #3 sectioned along a diameter.

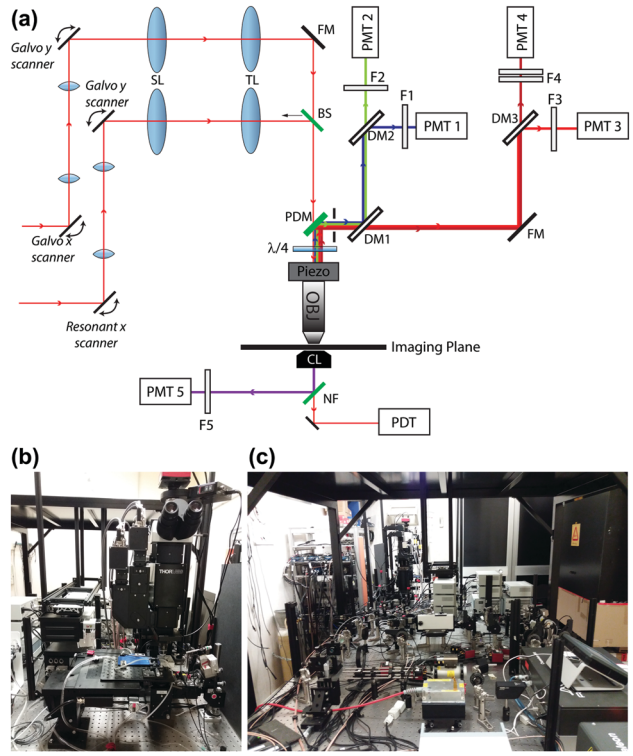

Fig. 2 Simplified optical scheme and actual photographs of the multiphoton microscope. (a) Red lines entering from the left represent titanium–sapphire (Ti:Sa) laser beams impinging on the pair of scanning systems. SL: scan lens; TL: tube lens; FM: full mirror; BS: 50/50 beam splitter; PDM: primary dichroic mirror; $\lambda/4$: quarter wave plate; Piezo: Piezo objective scanner; Obj: objective; DM1: 565 nm long pass filter (T565lpxr); DM2: 495 nm long pass filter (T495lpxru); DM3: 652 long pass filter (FF652-Di01-25x36); F1: 460/50 nm band pass filter (ET460/50m-2p); F2: 525/40 nm band pass filter (FF02-525/40-25); F3: 612/69 band pass filter (FF01-612/69-25); F4: combination of 647 nm long pass filter (BLP01-647R-25) and 770 nm short pass filter (FF01-770/SP-25); NF: notch filter; PMT: photomultiplier tube; PDT: photodiode tube. (b) Microscope front view. (c) Rear view.

locked titanium–sapphire (Ti:Sa) fs pulsed laser (Chameleon Vision II Laser, Coherent, Inc., Santa Clara, CA, USA). The RG scanner was used for imaging, whereas the GG scanner was used to focally photodamage a pre-defined spot in the GER of the cochlea by focusing the collimated laser beam onto the sample through a 25× water-immersion objective (XLPLN25XWMP2, NA 1.05, Olympus Corporation, Tokyo, Japan; the same objective was also used to image both preparations). Multiphoton excitation of Fluo 8H™ was performed at 920 nm, whereas its emission signal was filtered in the range 505–545 nm by a single band-pass filter (Cat. No. FF02-525/40-25, Semrock/IDEX, Rochester, NY, USA) placed in front of a non-descanned GaAsP detector (Cat. No. H7422-50, Hamamatsu Photonics K.K., Shizuoka, Japan, Fig. 2). Electro-optical modulators (EOM) and mechanical ultra-fast shutters were used to control both photodamage light dose (920 nm, power 150 mW, 100 ms) and imaging light exposure using the ThorImage LS 3.1 software (Thorlabs). Sequences of 512 × 512 pixel-frames were acquired at a final rate of 1 frame per second (after frame averaging) by oscillating the objective between the focal planes of the COC and ATP-WCBs (separated by a distance comprised between 20 μm and 100 μm, average 50 μm) using a piezo-electric actuator and paired controller (PFM450, Thorlabs). Laser excitation intensity and frame averaging were adjusted to minimize photobleaching and phototoxicity, while achieving enough signal to noise ratio and temporal resolution. All experiments were performed at room temperature (22–25 °C).

Luciferin–luciferase ATP bioluminescence assay

After overnight incubation under standard culture conditions (37 °C, 5% CO_2), COCs plated onto 5 mm glass coverslips were transferred into a black 96-well plate containing 200 μl serum-free DMEM/F12 in each well. Before starting the ATP release-stimulation protocol, COCs were washed once with a solution (NCS) containing a normal (1.8 mM) extracellular Ca^{2+} concentration and (in mM): 137 NaCl, 5.36 KCl, 0.81 $MgSO_4$, 0.44 KH_2PO_4, 0.18 Na_2HPO_4, 25 HEPES and 5.55 D-glucose (pH 7.3). COCs were then washed a second time either with NCS or with a zero Ca^{2+} solution (ZCS) containing (in mM): 137 NaCl, 5.36 KCl, 0.44 KH_2PO_4, 0.18 Na_2HPO_4, 0.1 EGTA, 25 HEPES and 5.55 D-glucose (pH 7.3).

To quantify ATP release, COCs were incubated in either NCS or ZCS for 20 minutes at 37 °C, 5% CO_2. To limit degradation of the released ATP, both solutions were supplemented with ARL67156 at a final concentration of 100 μM. The amount of ATP released under these conditions was measured with a bioluminescent ATP assay kit (Cat. No. A22066, ThermoFisher Scientific) using a luminometer (Victor Light 1420, Perkin Elmer, Waltham, MA, USA). All bioluminescence measurements reported in this article fell within the linearity range of the ATP standard curve generated according to the manufacturer's instructions. All experiments were performed at room temperature (22–25 °C).

Image processing and data analysis

Image processing and data analysis were carried out using the open source ImageJ software and MATLAB (R2019, The MathWorks, Inc., Natick, MA, USA). Ca^{2+} signals were quantified either as pixel-by-pixel relative changes of fluorescence emission intensity $\Delta F(t)$, where t is time, $F(t)$ is fluorescence at time t, $\Delta F(t) = F(t) - F_0$ and F_0 is the pre-stimulus fluorescence,[58] or as $100 \times \Delta F(t)/(F_{max} - F_0)$ where $F_{max} = \max[F(t)]$ during the time interval of the recording.

Statistics

For statistical data analysis, the normality of distribution was assayed using the Kolmogorov–Smirnov test and statistical comparisons of means were made using the Student t test. The Mann–Whitney U test was used for data which were not normally distributed and/or had dissimilar variance. All statistical analyses were performed using MATLAB (R2019). Mean values are quoted ± standard error of the mean (s.e.m.)

where p = p-value < 0.05 was assumed as statistically significant.

Results

Sensitivity of ATP-WCBs to ATP

To characterize the sensitivity of ATP-WCBs to ATP, we loaded cells with Ca^{2+} selective dyes and measured fluorescence intensity changes (ΔF) evoked by different [ATP] in the range from 0.1 nM to 1 μM (see Methods). Fig. 3a shows dose–response data fitted with a Hill function

$$\frac{\Delta F}{\Delta F_{sat}} = \left(1 + \frac{EC_{50}}{[ATP]}\right)^{-1} \quad (1)$$

where ΔF_{sat} is the value attained by ΔF at saturating values of the [ATP]. The fit yielded a half-maximal effective concentration (EC_{50} = 6.2 nM) very close to the baseline [ATP] in the endolymph.[28,29] Ca^{2+} signals evoked by 100 nM [ATP] (a nearly saturating concentration, see Fig. 3a and b) were dramatically reduced after 30 min of incubation with suramin (150 μM, Fig. 3c), a reversible $P2Y_2R$ antagonist.[59–61] The ATP-evoked ΔF signal, integrated over time and averaged over the population of ATP-WCBs, increased 30-fold after drug wash out (Fig. 3c and d). We note in passing that parental HEK293-T cells, from which these ATP-WCBs were derived, are very weakly coupled through gap junction channels composed of Cx43 subunits;[62] therefore the observed Ca^{2+} signals were independent of the confluence state and reflected individual cell responses to the proximal [ATP].

Solving eqn (1) for [ATP] with EC_{50} = 6.2 nM yields

$$[ATP] = (6.2\ \mathrm{nM})\left(\frac{\Delta F_{sat}}{\Delta F} - 1\right)^{-1} \quad (2)$$

which can be used to estimate [ATP] in the proximity of the ATP-WCBs from the measurement of ΔF and ΔF_{sat}.

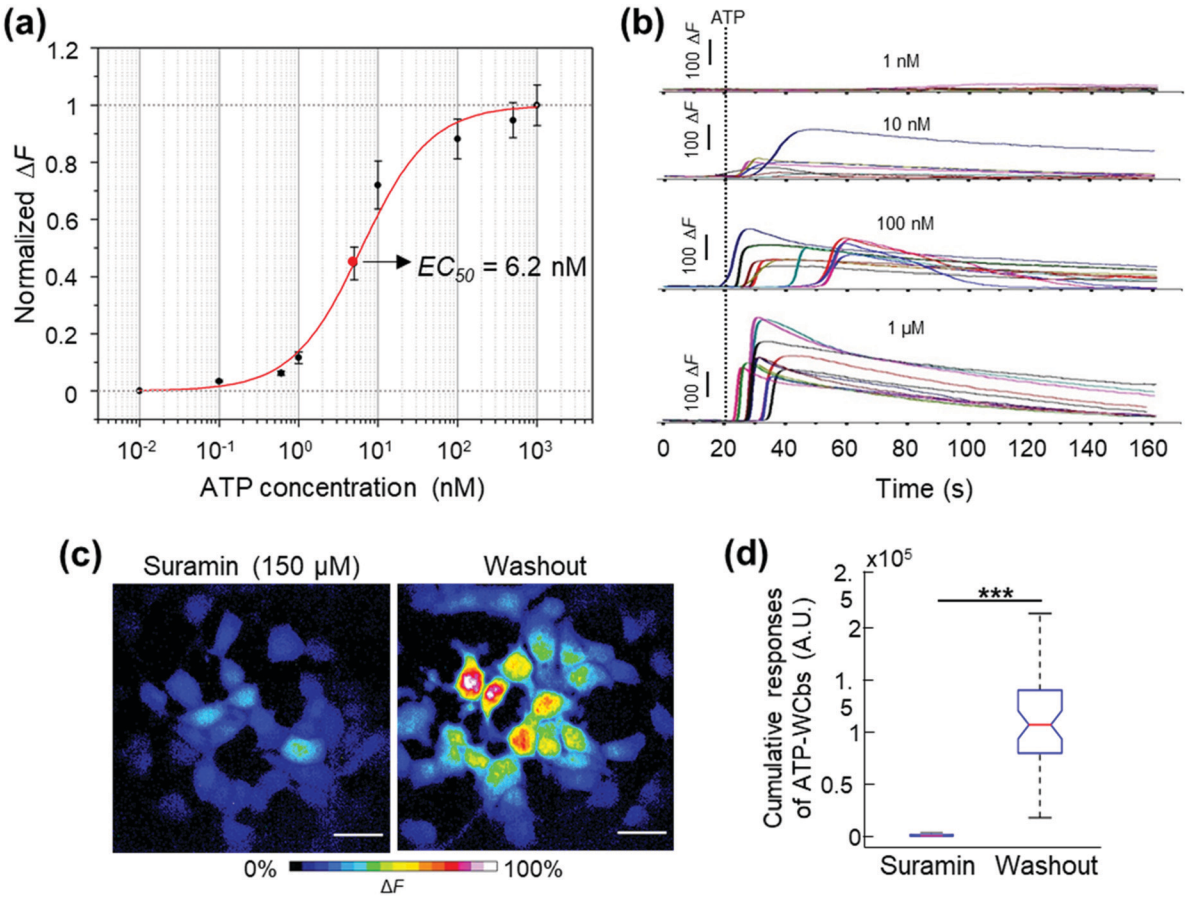

Fig. 3 Ca^{2+} responses of ATP-WCBs evoked by exogenously applied ATP. (a) Each data point is the mean Ca^{2+}-dependent fluorescence change $\Delta F/F_{sat}$ ± s.e.m. for n = 8 wells of a 96-well plate. Each well contained ATP-WCBs seeded at a density of 1×10^5 cells per cm^2 and loaded with the FLIPR Calcium 6 Assay Kit (see Methods). The solid line is a fit with the Hill function described in the main text. (b) Representative traces showing ATP-evoked Ca^{2+} responses in individual ATP-WCBs loaded with Fluo8H™; each trace was generated as the pixel average of ΔF signals in a region of interest (ROI) encompassing a responding cell. (c) Shown are pseudo-color images acquired using the spinning disk confocal fluorescence microscope (see Methods) and representing percent fluorescence changes, encoded as shown by the color scale bar, evoked by 100 nM ATP; each image is the maximal projection rendering of all frames in a sequence of 490 fluorescence images acquired at 4 frames per second (f.p.s.) after 30 minutes of incubation with suramin (150 μM, left) and after washout (right); scale bars: 30 μm. (d) Box plots represent distributions of ΔF signals integrated over time in n = 49 ATP-WCBs from the experiments in (c) (***, $p < 0.001$; Mann–Whitney U test; a.u., arbitrary units).

Together, these experiments suggested that ATP-WCBs, if placed sufficiently close to the ATP source in a suitable environment, had the required sensitivity to detect physiologically relevant levels of ATP.

Design, construction and test of a microfluidic chamber suitable to detect ATP release from COCs

To determine whether ATP-WCBs responded to the ATP released in the extracellular medium by COCs, we exploited the intrinsic optical sectioning capabilities of multiphoton microscopy[63] and performed dual focal plane Ca^{2+} imaging in an *ad hoc* designed, closed and transparent micro-fluidic chamber hosting ATP-WCBs at the top and a proximally located COC at the bottom (see Methods and Fig. 1 and 2). To increase detection sensitivity, hydrolysis of ATP was reduced by supplementing the extracellular medium with ARL67156 (100 μM), a widely used ectonucleotidase inhibitor.[64,65]

Initially, we used the second scanning head and fast beam shuttering of the multiphoton microscope (Fig. 2) to rapidly photodamage a single GER cell (see Methods) in COCs from wild type C57BL6/N pups, resulting in the time-controlled spreading of a Ca^{2+} wave around the damage spot (Fig. 4a and Video S1 in the ESI‡). The overlying ATP-WCBs in the microfluidic chamber responded with clearly detectable and time-delayed Ca^{2+} signals (n = 3 out of 3 independent experiments). No signal was detected in ATP-WCBs if the same procedure was performed without including a COC in the chamber (n = 3 independent experiments), indicating that the observed responses were not due to photodamage of ATP-WCBs or other spurious effects.

Replacing ARL67156 in the extracellular medium with apyrase (40 U ml^{-1}), an ATP-hydrolyzing enzyme,[66] caused a dramatic reduction of Ca^{2+} wave amplitude and extent in COCs. Ca^{2+} responses in the overlying ATP-WCBs were correspondingly reduced, confirming that they were due to the diffusion of the released ATP in the narrow fluid gap (20–100 μm) intercalated between the two cellular systems. For the representative experiment in Fig. 4b, the responses, integrated over time and summed over all ATP-WCBs within the field of view, were 3.36 × 10^6 A.U. in the presence of ARL67156 *vs.* 7.00 × 10^4 A.U. in the presence of apyrase (a 48-fold reduction). By using eqn (2) to estimate the average [ATP] that reached ATP-WCBs in the presence of ARL67156, we obtained values in the range from 5 nM to 48 nM. Similar results were obtained in two other independent experiments.

Together, these results suggested that ATP-WCBs in the microfluidic chamber could detect ATP release during stimulated Ca^{2+} wave propagation in the GER.

Analysis of spontaneous Ca^{2+} wave propagation and ATP release from the GER of genetically modified mice by dual multiphoton imaging in the microfluidic chamber

Based on the positive outcomes of the aforementioned experiments, we decided to investigate spontaneous Ca^{2+} wave propagation in the GER of pups with global deletion of *Panx1* (Fig. 5 and Video S2 in the ESI‡) or *Gjb6* (Fig. 6 and Video S3 in the ESI‡) using the microfluidic chamber. The distributions of ATP-WCB Ca^{2+} responses, integrated over time and driven by spontaneous Ca^{2+} wave propagation in the underlying GER from *Panx1*$^{-/-}$ and *Panx1*$^{+/+}$ COCs, were statistically indistinguishable (Fig. 7a: *Panx1*$^{-/-}$: mean = 2.38 × 10^4, median = 7.33 × 10^3, I.Q.R. = 2.19 × 10^4 A.U.; *Panx1*$^{+/+}$: mean = 2.07 × 10^4 A.U., median = 3.88 × 10^3, I.Q.R. = 1.74 × 10^4 A.U.; m = 1695 ATP-WCBs in each case; p = 0.105, Mann–Whitney U test; pooled results from n = 7 pups

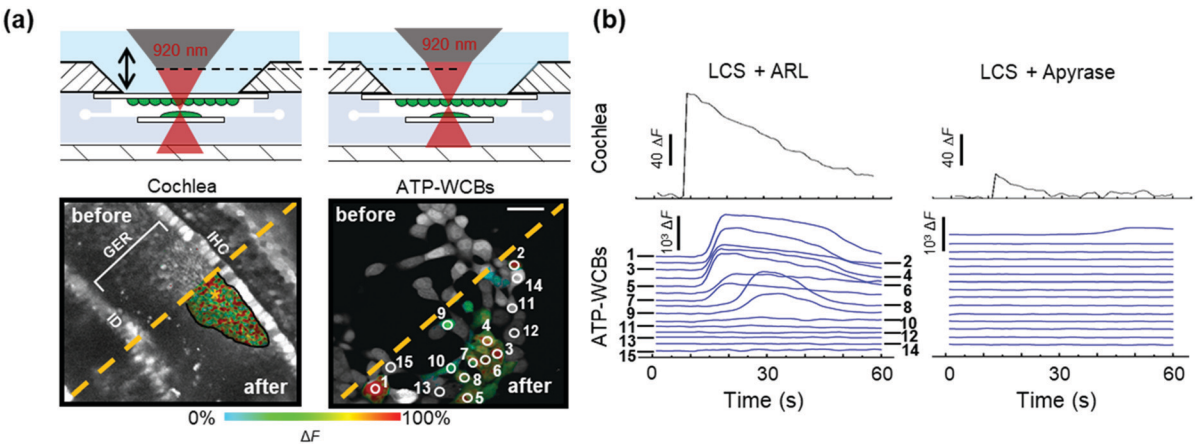

Fig. 4 Ca^{2+} responses of ATP-WCBs evoked by photodamaging a single GER cell in an underlying wild type (C57BL6/N) COC within the microfluidic chamber. (a) Top: Schematic representation of the microfluidic chamber (filled with LCS and) containing COC and ATP-WCBs facing one another in focal planes that were distinguished by the intrinsic optical sectioning capabilities of multiphoton confocal microscopy; bottom: Fluo 8H™ confocal images acquired from the two focal planes (left: COC; right: ATP-WCBs) before and after photodamaging a single GER cell (marked by the yellow asterisk); scale bar: 50 μm. (b) Top: ΔF signals generated as pixel average from all cells of the COC that responded to the focal photodamage event; bottom: representative ΔF signals detected in individual ATP-WCBs overlying the COC.

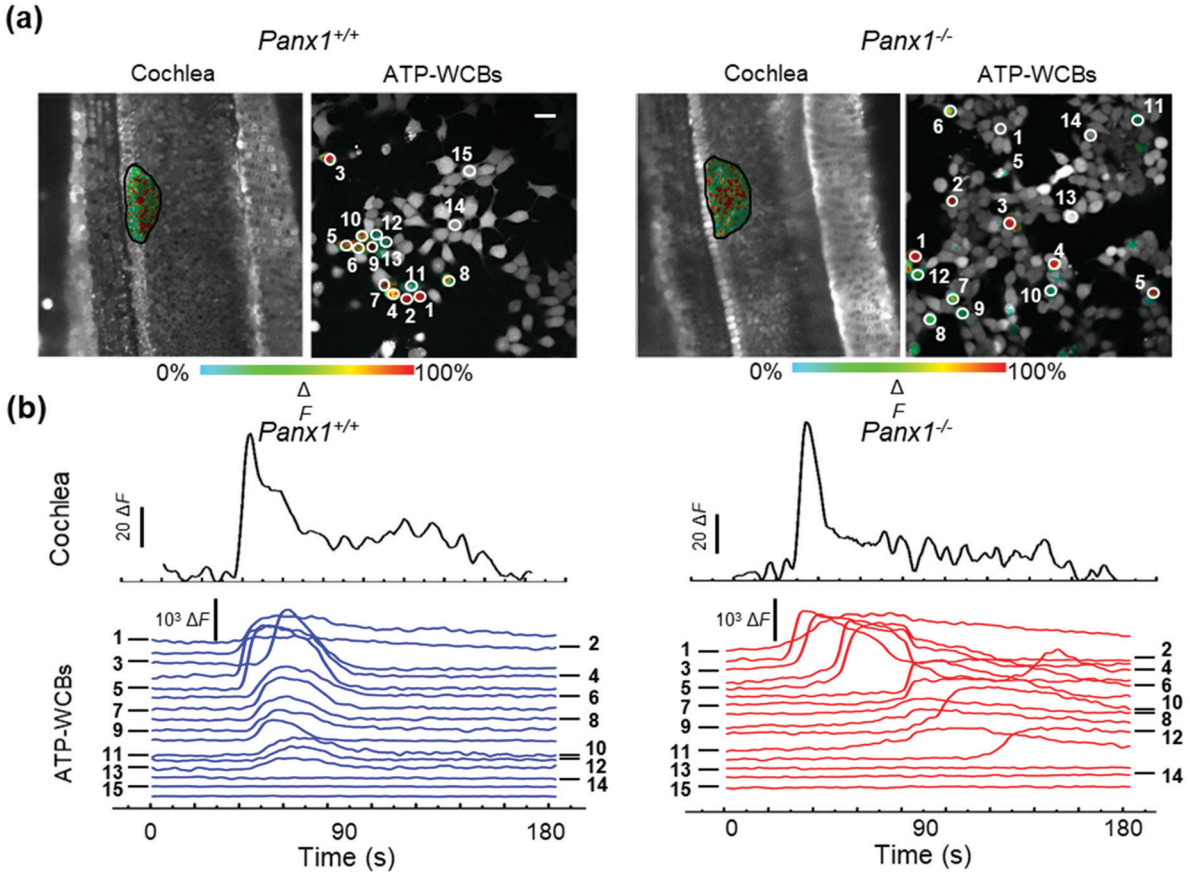

Fig. 5 Ca^{2+} responses of ATP-WCBs evoked by ATP release in the microfluidic chamber during spontaneous Ca^{2+} wave propagation in underlying COCs from pups with global deletion of *Panx1* (*Panx1*$^{-/-}$) and their siblings with normal *Panx1* alleles (*Panx1*$^{+/+}$). (a) Representative multiphoton confocal fluorescence images showing the occurrence of a spontaneous Ca^{2+} wave in non-sensory cells of the GER and corresponding ATP-WCB responses; scale bars: 50 μm. (b) Top (black traces): ΔF signals generated as pixel average from all cells of the GER reached by the shown spontaneous Ca^{2+} wave; bottom (blue and red traces): representative ΔF signals detected in individual ATP-WCBs in response to the underlying Ca^{2+} wave in the GER.

of each genotype). By using eqn (2) to estimate the average [ATP] near ATP-WCBs, we obtained values in the range from 7 nM to 30 nM for *Panx1*$^{-/-}$ as well as *Panx1*$^{+/+}$ COCs.

In prior work, the frequency of GER spontaneous Ca^{2+} waves was dramatically reduced in *Gjb6*$^{-/-}$ animals compared to their siblings with normal *Gjb6* alleles (*Gjb6*$^{+/+}$).[18,20] Here, in addition, we report significantly different distributions of Ca^{2+} responses obtained from ATP-WCBs overlying *Gjb6*$^{-/-}$ COCs in the microfluidic chamber (Fig. 7b; mean = 2.90 × 10^3, median = 460, I.Q.R. = 1.97 × 10^3 A.U.) *vs.* *Gjb61*$^{+/+}$ COCs (mean = 2.30 × 10^4, median = 2.59 × 10^3, I.Q.R. = 1.67 × 10^4 A.U.; m = 606 ATP-WCBs in each case; p = 3.04 × 10^{-27}, Mann–Whitney U test; pooled results from n = 4 pups of each genotype, aged P5).

Independent estimate of ATP release from *Panx1*$^{-/-}$ and Cx30$^{-/-}$ cochlear organotypic cultures

As an additional control, we used also a standard luciferin–luciferase ATP bioluminescence assay[67] to measure ATP release from COCs in 96-well plates (see Methods). In COCs obtained from *Panx1*$^{+/+}$ and *Panx1*$^{-/-}$ P5 pups, ATP release was equally enhanced by lowering the concentration of extracellular Ca^{2+} from 1.8 mM (NCS) to 0 mM (ZCS), a procedure that increases the open probability of connexin hemichannels[68] without affecting pannexin channels.[69–71] Specifically, the amount of ATP released in the extracellular medium in ZCS was 205% ± 30% of the NCS control in *Panx1*$^{-/-}$ COCs (p = 0.015, t test) and 268% ± 54% in *Panx1*$^{+/+}$ COCs (p = 0.011, t test). The ATP released in the extracellular medium was not significantly different between the two genotypes, either in ZCS (p = 0.265, t test) or in NCS (p = 0.93, t test, n = 6 cultures of either genotype; Fig. 8a). In contrast, the ATP released in the extracellular medium in ZCS was 225% ± 18% of the NCS control in *Gjb6*$^{-/-}$ COCs (p = 0.0001, t test) and 145% ± 16% in *Gjb6*$^{+/+}$ COCs (p = 0.074). In this case, the amount of released ATP in ZCS was significantly different between the two genotypes (p = 0.001, t test; Fig. 8b).

Together, the results of Fig. 4–8 indicate that: (i) ATP-WCBs in the microfluidic environment had the required

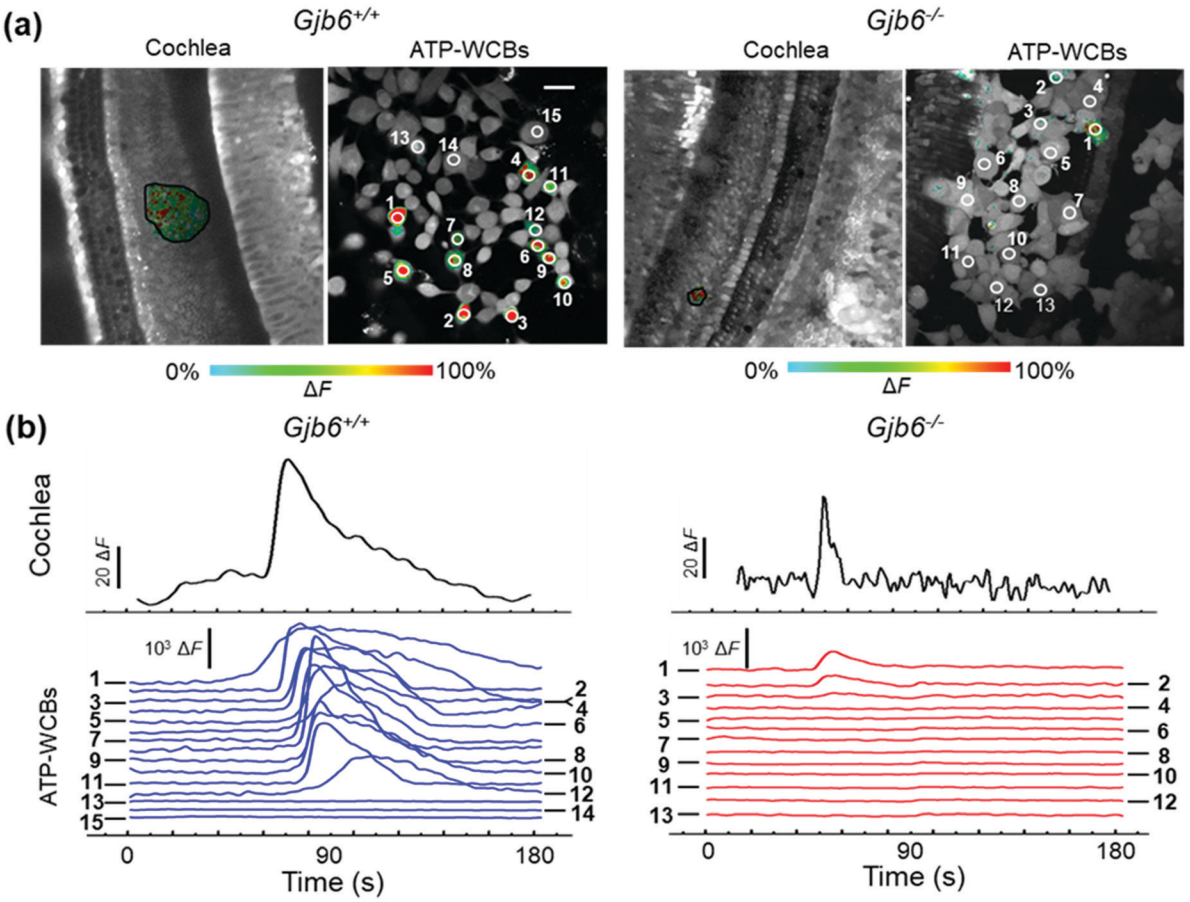

Fig. 6 Ca^{2+} responses of ATP-WCBs evoked by ATP release in the microfluidic chamber during spontaneous Ca^{2+} wave propagation in underlying COC from pups with global deletion of *Gjb6* (*Gjb6*$^{-/-}$) and their siblings with normal *Gjb6* alleles (*Gjb6*$^{+/+}$). (a) Representative multiphoton confocal fluorescence images showing the occurrence of a spontaneous Ca^{2+} wave in non-sensory cells of the GER and corresponding ATP-WCB responses; scale bars: 50 μm. (b) Top (black traces): ΔF signals generated as pixel average from all cells of the GER reached by the shown spontaneous Ca^{2+} wave; bottom (blue and red traces): representative ΔF signals detected in individual ATP-WCBs in response to the underlying Ca^{2+} wave in the GER.

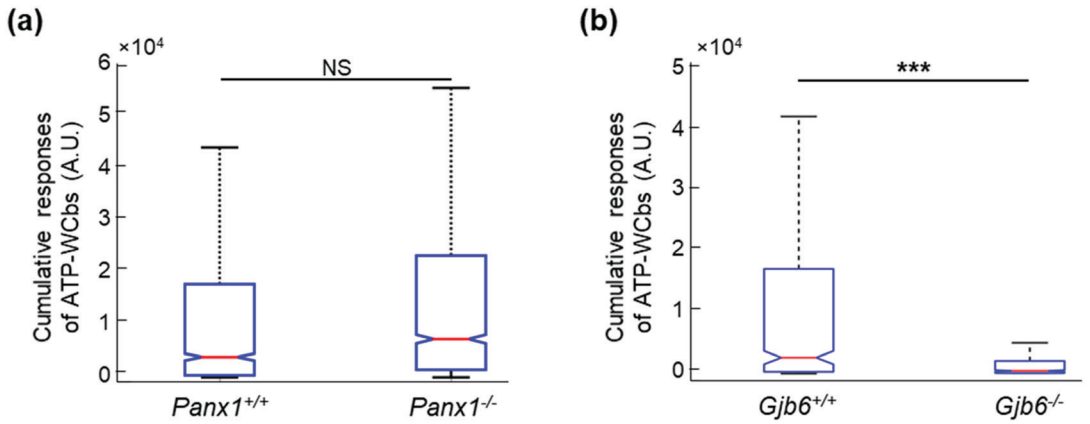

Fig. 7 Box plots showing the distributions of ATP-WCB responses in the microfluidic chamber integrated over time and driven by spontaneous Ca^{2+} wave propagation in the underlying GER from (a) *Panx1*$^{+/+}$ or *Panx1*$^{-/-}$ pups (n = 1695 cells ATP-WCBs in each case) and (b) *Gjb6*$^{+/+}$ or *Gjb6*$^{-/-}$ pups (n = 606 cells in each case); ***, $p < 0.001$; NS, not significant; Mann–Whitney U test.

sensitivity to detect the ATP released by stimulated as well as spontaneous Ca^{2+} wave propagation in the GER; (ii) ATP release was unaffected by *Panx1* genetic ablation (iii) but strongly reduced by *Gjb6* ablation.

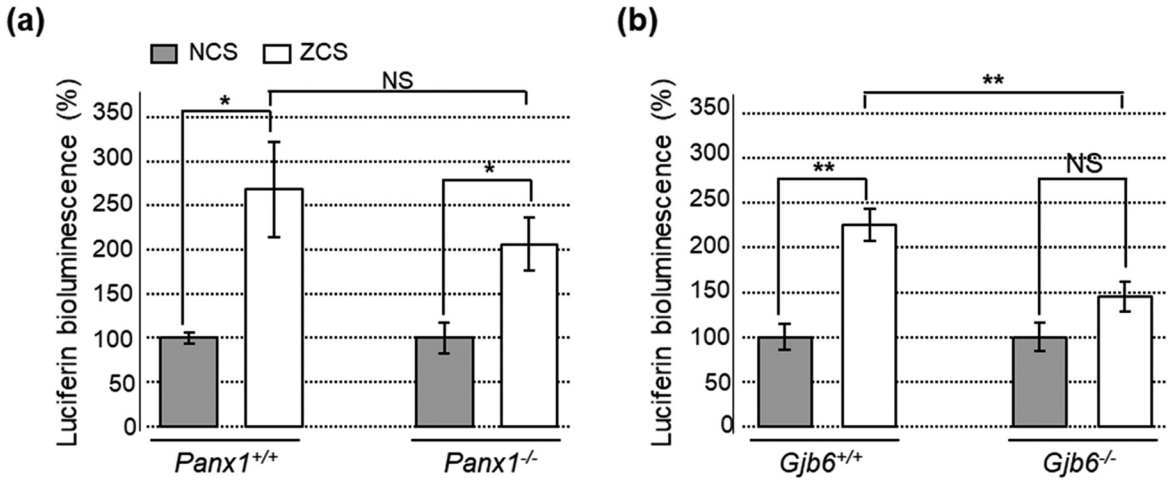

Fig. 8 Luciferin–luciferase ATP bioluminescence assay of ATP release in COCs from *Panx1*$^{-/-}$ and *Gjb6*$^{-/-}$ mouse pups. Histograms represent mean bioluminescence values ± s.e.m. normalized to corresponding values in control COCs (*Panx1*$^{+/+}$ and *Gjb6*$^{+/+}$, respectively). Data were obtained in n = 6 COCs from 6 different animals for each genotype. NCS, normal (1.8 mM) Ca^{2+} saline solution; ZCS, 0 mM Ca^{2+} saline solution. Asterisks indicate the significance level relative to controls (*, $p < 0.05$; **, $p < 0.01$; NS, $p > 0.5$, t test).

Discussion and conclusions

Prior work has unveiled a critical role for connexin hemichannels in Ca^{2+} wave propagation in both the LER[25–27] and the GER.[17,18,22] The goal of this work was to determine whether ATP release through connexin hemichannels underlies Ca^{2+} wave propagation also in the GER of the developing cochlea (rather than only in the LER, as abundantly documented). To address this key issue, we used microfluidics, which is capable of manipulating cells and organ models in a highly controllable microenvironment (Fig. 1), coupled with multiphoton imaging (Fig. 2). This disruptive combination of key enabling technologies is creating breakthroughs in current understanding of cell and developmental biology and is providing insights into disease diagnosis in numerous fields.[72]

WCBs were the third essential element of our design (Fig. 3). For more than a quarter century, WCBs have provided critical insight into the physiological effect of numerous analytes (reviewed in ref. 43, 73 and 74). To create ATP-WCBs, we infected HEK-293T cells with a lentiviral vector encoding the highly sensitive $P2Y_2R$, one of the two major P2Y receptors expressed in the developing cochlea.[3,6] The binding of ATP to $P2Y_2R$ promotes the generation of diacylglycerol and $InsP_3$ from PLC-dependent hydrolysis of PIP_2.[18] Intracellular diffusion of $InsP_3$ and subsequent binding to $InsP_3$ receptors triggers Ca^{2+} release from the endoplasmic reticulum (ER), increasing the cytosolic Ca^{2+} concentration.[75] By optically monitoring these Ca^{2+} fluctuations with Ca^{2+}-selective dyes,[58] we determined that our ATP-WCBs had the required sensitivity to detect [ATP] fluctuations in the sub-micromolar range, with EC_{50} close to the baseline [ATP] measured in the rodent endolymph *in vivo*.[28,29]

By oscillating the objective of the multiphoton microscope between the focal planes of COC and overlying ATP-WCBs in the microfluidic chamber, we correlated [ATP]-dependent Ca^{2+} fluctuations in ATP-WCBs to stimulated (Fig. 4) as well as spontaneous Ca^{2+} wave propagation in the GER of genetically modified mice (Fig. 5 and 6). Ca^{2+} signals where inhibited by apyrase, as previously reported for ATP-dependent Ca^{2+} wave propagation in the LER of wild type mice.[4] Importantly, spontaneous Ca^{2+} wave propagation in the GER resulted in time-delayed ATP-WCB responses that were strongly reduced by global deletion of *Gjb6*, but unaffected by global deletion of *Panx1* (Fig. 7). Quantification of ATP release from COCs by means of a standard luciferin–luciferase bioluminescence assay corroborated this conclusion (Fig. 8). However, the luciferin-luciferase approach, the main strategy to measure ATP nowadays, which focuses on supernatants, falls short of providing the kind of information that is made available by our organ-on-chip/ATP-WCBs system and optical technology.

Although pannexin 1 channels[71] are thought to mediate ATP release in other cellular systems,[76–81] the function of cochlear pannexins remains obscure.[34,82–84] Prior work with the *Panx1*$^{-/-}$ strain used here confirmed (i) successful ablation of *Panx1* both in the cochlea and in the brain; (ii) normal hearing sensitivity, normal function of the outer hair cell-based "cochlear amplifier" and absence of cochlear nerve defects; (iii) normal expression of inner ear connexins and gap junction communication in the organ of Corti.[34] These published results and the data presented here together rule out that pannexin 1 channels contribute to the purinergic signaling that underlies Ca^{2+} wave propagation in the developing cochlea.[2]

Gjb6$^{-/-}$ mice, in which Cx30 is deleted globally[38] and Cx26 is dramatically down-regulated in the sensory epithelium of the developing cochlea,[33] are a model of non-syndromic hearing loss and deafness (DFNB1, reviewed in ref. 37 and 85). Prior work revealed impaired Ca^{2+} wave propagation in the developing cochlea of these mice,[18,33] which could be

restored by viral transduction with a bovine adeno-associated vector (BAAV) encoding Cx30.[18,86] The expression of connexin hemichannels at the endolymphatic surface of the cochlear sensory epithelium has been confirmed by immunolabeling with antibodies that bind the extracellular loops of Cx26 and Cx30.[25,26,87] In addition, spontaneous Ca^{2+} wave propagation at the surface of the GER was inhibited by (i) flufenamic acid (FFA),[17,18,22] a nonspecific blocker of connexin hemichannels[88,89] which, unlike carbenoxolone,[90] is ineffective on pannexin 1 channels at concentrations <300 μM (ref. 80 and 91) and (ii) the abEC1.1 antibody, which does not interfere with pannexin 1 channels, is selective for Cx26, Cx30 and Cx32 hemichannels, reduces connexin hemichannel currents and abrogates ATP release.[35,36,92] This vast body of experimental results, together with the data presented here, demonstrate that ATP-dependent ATP release through connexin hemichannels sustains Ca^{2+} wave propagation not only in the LER,[25–27] but also in the GER.

The ATP released during Ca^{2+} wave propagation in the GER has been proposed to trigger Ca^{2+} action potential (AP) activity in immature IHCs, driving bursts of APs in the auditory nerve fibers.[14] However, subsequent work has shown AP firing in the complete absence of Ca^{2+} activity in the GER.[20] Therefore, it remains to be established if and how these two types of spontaneous activities correlate with each other. This stands out a key open question for cochlear physiopathology, as connexin expression and spontaneous Ca^{2+} signaling in the GER are essential for normal development of the sensory epithelium, hair cell functional maturation, hearing acquisition,[20–23] redox homeostasis and age-related hearing loss.[24] We are confident that the technological advances presented here have the potential to shed light on this as well as a plethora of other unrelated open issues that concern the role of paracrine signaling in physiology and pathology[93] and cannot be addressed with standard methods.

Author contributions

Conceptualization, F. M. (Fabio Mammano); methodology, F. M., Fl. M. (Flavia Mazzarda), A. D'E., R. M., A. D. N., F. R. B., A. T. M., L. B., F. C.; resources F. M., F. R. B., L. B., A. S., M. R., F. S.; investigation, Fl. M., C. P., G. Z., V. Z., C. N.; formal analysis, data curation, visualization and writing—original draft preparation, Fl. M.; supervision, writing—review and editing, project administration and funding acquisition A. M. S., M. R., J. Y., F. M. All the authors have read and agreed to the published version of the manuscript.

Conflicts of interest

The authors declare no conflict of interest. The funders had no role in the design of the study, in the collection, analyses, or interpretation of data, in the writing of the manuscript, or in the decision to publish the results.

Acknowledgements

This project has received funding from Fondazione Telethon (grant GGP13114), the National Research Council of Italy (CNR) Grant No. DSB.AD008.370.003\TERABIO-IBCN and the University of Padova Grant SID\BIRD187130 to F. M., and from the Italian Ministry of Research and University, grant PRIN 2017FTJ5ZE Sensory decay and aging to M. R. The authors thank Mr. Fabrizio Bonaventura for technical assistance, as well as Prof. Mario Bortolozzi and two anonymous reviewers for constructive criticism and helpful suggestions.

References

1 G. D. Housley, A. Bringmann and A. Reichenbach, *Trends Neurosci.*, 2009, **32**, 128–141.
2 F. Mammano, *Semin. Cell Dev. Biol.*, 2013, **24**, 31–39.
3 E. Berekmeri, J. Szepesy, L. Koles and T. Zelles, *Brain Res. Bull.*, 2019, **151**, 109–118.
4 J. E. Gale, V. Piazza, C. D. Ciubotaru and F. Mammano, *Curr. Biol.*, 2004, **14**, 526–529.
5 M. Beltramello, V. Piazza, F. F. Bukauskas, T. Pozzan and F. Mammano, *Nat. Cell Biol.*, 2005, **7**, 63–69.
6 V. Piazza, C. D. Ciubotaru, J. E. Gale and F. Mammano, *Cell Calcium*, 2007, **41**, 77–86.
7 D. J. Lim and M. Anniko, *Acta Oto-Laryngol., Suppl.*, 1985, **422**, 1–69.
8 D. J. Lim and J. Rueda, in *Development of auditory and vestibular systems - 2*, ed. R. Romand, Elsevier Science Publishing Co., New York, 1st edn, 1992, pp. 33–58.
9 A. A. Eggston and D. Wolff, in *Histopathology of the ear, nose, and throat*, Williams and Wilkins Co., Baltimore, 1947, pp. 37–64.
10 R. Hinojosa, *Acta Oto-Laryngol.*, 1977, **84**, 238–251.
11 S. Hou, J. Chen and J. Yang, *Eur. J. Histochem.*, 2019, **63**, 102–109.
12 M. W. Kelley, *Int. J. Dev. Biol.*, 2007, **51**, 571–583.
13 J. Bryant, R. J. Goodyear and G. P. Richardson, *Br. Med. Bull.*, 2002, **63**, 39–57.
14 N. X. Tritsch, E. Yi, J. E. Gale, E. Glowatzki and D. E. Bergles, *Nature*, 2007, **450**, 50–55.
15 N. X. Tritsch, Y. X. Zhang, G. Ellis-Davies and D. E. Bergles, *Purinergic Signalling*, 2010, **6**, 155–166.
16 H. C. Wang, C. C. Lin, R. Cheung, Y. Zhang-Hooks, A. Agarwal, G. Ellis-Davies, J. Rock and D. E. Bergles, *Cell*, 2015, **163**, 1348–1359.
17 M. Schutz, P. Scimemi, P. Majumder, R. D. De Siati, G. Crispino, L. Rodriguez, M. Bortolozzi, R. Santarelli, A. Seydel, S. Sonntag, N. Ingham, K. P. Steel, K. Willecke and F. Mammano, *Hum. Mol. Genet.*, 2010, **19**, 4759–4773.
18 L. Rodriguez, E. Simeonato, P. Scimemi, F. Anselmi, B. Cali, G. Crispino, C. D. Ciubotaru, M. Bortolozzi, F. G. Ramirez, P. Majumder, E. Arslan, P. De Camilli, T. Pozzan and F. Mammano, *Proc. Natl. Acad. Sci. U. S. A.*, 2012, **109**, 14013–14018.
19 T. Eckrich, K. Blum, I. Milenkovic and J. Engel, *Front. Mol. Neurosci.*, 2018, **11**, 264–264.

20 S. L. Johnson, F. Ceriani, O. Houston, R. Polishchuk, E. Polishchuk, G. Crispino, V. Zorzi, F. Mammano and W. Marcotti, *Journal of Neuroscience*, 2017, **37**, 258–268.
21 F. Ceriani, A. Hendry, J. Y. Jeng, S. L. Johnson, F. Stephani, J. Olt, M. C. Holley, F. Mammano, J. Engel, C. J. Kros, D. D. Simmons and W. Marcotti, *EMBO J.*, 2019, **38**(9), e99839.
22 F. Mammano and M. Bortolozzi, *Cell Calcium*, 2018, **70**, 117–126.
23 G. Crispino, G. Di Pasquale, P. Scimemi, L. Rodriguez, F. Galindo Ramirez, R. D. De Siati, R. M. Santarelli, E. Arslan, M. Bortolozzi, J. A. Chiorini and F. Mammano, *PLoS One*, 2011, **6**, e23279.
24 A. R. Fetoni, V. Zorzi, F. Paciello, G. Ziraldo, C. Peres, M. Raspa, F. Scavizzi, A. M. Salvatore, G. Crispino, G. Tognola, G. Gentile, A. G. Spampinato, D. Cuccaro, M. Guarnaccia, G. Morello, G. Van Camp, E. Fransen, M. Brumat, G. Girotto, G. Paludetti, P. Gasparini, S. Cavallaro and F. Mammano, *Redox Biol.*, 2018, **19**, 301–317.
25 F. Anselmi, V. H. Hernandez, G. Crispino, A. Seydel, S. Ortolano, S. D. Roper, N. Kessaris, W. Richardson, G. Rickheit, M. A. Filippov, H. Monyer and F. Mammano, *Proc. Natl. Acad. Sci. U. S. A.*, 2008, **105**, 18770–18775.
26 P. Majumder, G. Crispino, L. Rodriguez, C. D. Ciubotaru, F. Anselmi, V. Piazza, M. Bortolozzi and F. Mammano, *Purinergic Signalling*, 2010, **6**, 167–187.
27 F. Ceriani, T. Pozzan and F. Mammano, *Proc. Natl. Acad. Sci. U. S. A.*, 2016, **113**, E7194–E7201.
28 D. J. Munoz, P. R. Thorne, G. D. Housley and T. E. Billett, *Hear. Res.*, 1995, **90**, 119–125.
29 S. M. Vlajkovic, P. R. Thorne, G. D. Housley, D. J. Munoz and I. S. Kendrick, *NeuroReport*, 1998, **9**, 1559–1565.
30 J. Lautermann, H. G. Frank, K. Jahnke, O. Traub and E. Winterhager, *Dev. Genet.*, 1999, **25**, 306–311.
31 J. Lautermann, W. J. ten Cate, P. Altenhoff, R. Grummer, O. Traub, H. Frank, K. Jahnke and E. Winterhager, *Cell Tissue Res.*, 1998, **294**, 415–420.
32 A. Forge, D. Becker, S. Casalotti, J. Edwards, N. Marziano and G. Nevill, *J. Comp. Neurol.*, 2003, **467**, 207–231.
33 S. Ortolano, G. Di Pasquale, G. Crispino, F. Anselmi, F. Mammano and J. A. Chiorini, *Proc. Natl. Acad. Sci. U. S. A.*, 2008, **105**, 18776–18781.
34 V. Zorzi, F. Paciello, G. Ziraldo, C. Peres, F. Mazzarda, C. Nardin, M. Pasquini, F. Chiani, M. Raspa, F. Scavizzi, A. Carrer, G. Crispino, C. D. Ciubotaru, H. Monyer, A. R. Fetoni, A. M. Salvatore and F. Mammano, *Front. Mol. Neurosci.*, 2017, **10**, 379.
35 L. Xu, A. Carrer, F. Zonta, Z. Qu, P. Ma, S. Li, F. Ceriani, D. Buratto, G. Crispino, V. Zorzi, G. Ziraldo, F. Bruno, C. Nardin, C. Peres, F. Mazzarda, A. M. Salvatore, M. Raspa, F. Scavizzi, Y. Chu, S. Xie, X. Yang, J. Liao, X. Liu, W. Wang, S. Wang, G. Yang, R. A. Lerner and F. Mammano, *Front. Mol. Neurosci.*, 2017, **10**, 298.
36 G. Ziraldo, D. Buratto, Y. Kuang, L. Xu, A. Carrer, C. Nardin, F. Chiani, A. M. Salvatore, G. Paludetti, R. A. Lerner, G. Yang, F. Zonta and F. Mammano, *Front. Physiol.*, 2019, **10**, 392.
37 F. Mammano, *Cold Spring Harbor Perspect. Med.*, 2019, **9**(7), a033233.
38 B. Teubner, V. Michel, J. Pesch, J. Lautermann, M. Cohen-Salmon, G. Sohl, K. Jahnke, E. Winterhager, C. Herberhold, J. P. Hardelin, C. Petit and K. Willecke, *Hum. Mol. Genet.*, 2003, **12**, 13–21.
39 M. Cohen-Salmon, B. Regnault, N. Cayet, D. Caille, K. Demuth, J. P. Hardelin, N. Janel, P. Meda and C. Petit, *Proc. Natl. Acad. Sci. U. S. A.*, 2007, **104**, 6229–6234.
40 Q. Chang, W. Tang, S. Ahmad, B. Zhou and X. Lin, *PLoS One*, 2008, **3**, e4088.
41 P. Bargiotas, A. Krenz, S. G. Hormuzdi, D. A. Ridder, A. Herb, W. Barakat, S. Penuela, J. von Engelhardt, H. Monyer and M. Schwaninger, *Proc. Natl. Acad. Sci. U. S. A.*, 2011, **108**, 20772–20777.
42 S. Petric, S. Klein, L. Dannenberg, T. Lahres, L. Clasen, K. G. Schmidt, Z. Ding and B. C. Donner, *Cell. Physiol. Biochem.*, 2016, **38**, 487–501.
43 Q. Gui, T. Lawson, S. Shan, L. Yan and Y. Liu, *Sensors*, 2017, **17**(7), pii: s17071623.
44 K. L. Kane, C. M. Longo-Guess, L. H. Gagnon, D. Ding, R. J. Salvi and K. R. Johnson, *Hear. Res.*, 2012, **283**, 80–88.
45 C. Kilkenny, W. J. Browne, I. C. Cuthill, M. Emerson and D. G. Altman, *PLoS Biol.*, 2010, **8**, e1000412.
46 A. J. Smith, R. E. Clutton, E. Lilley, K. E. A. Hansen and T. Brattelid, *Lab. Anim.*, 2018, **52**, 135–141.
47 S. Lemeshow, D. W. Hosmer, J. Klar and S. K. Lwanga, *Adequacy of sample size in health studies*, Wiley, New York, NY, USA, 1990.
48 M. P. Abbracchio, G. Burnstock, J. M. Boeynaems, E. A. Barnard, J. L. Boyer, C. Kennedy, G. E. Knight, M. Fumagalli, C. Gachet, K. A. Jacobson and G. A. Weisman, *Pharmacol. Rev.*, 2006, **58**, 281–341.
49 C. E. Parr, D. M. Sullivan, A. M. Paradiso, E. R. Lazarowski, L. H. Burch, J. C. Olsen, L. Erb, G. A. Weisman, R. C. Boucher and J. T. Turner, *Proc. Natl. Acad. Sci. U. S. A.*, 1994, **91**, 3275–3279.
50 D. G. Gibson, L. Young, R. Y. Chuang, J. C. Venter, C. A. Hutchison, 3rd and H. O. Smith, *Nat. Methods*, 2009, **6**, 343–345.
51 J. H. Kim, S. R. Lee, L. H. Li, H. J. Park, J. H. Park, K. Y. Lee, M. K. Kim, B. A. Shin and S. Y. Choi, *PLoS One*, 2011, **6**, e18556.
52 N. C. Shaner, M. Z. Lin, M. R. McKeown, P. A. Steinbach, K. L. Hazelwood, M. W. Davidson and R. Y. Tsien, *Nat. Methods*, 2008, **5**, 545–551.
53 M. Sena-Esteves and G. Gao, *Cold Spring Harb. Protoc.*, 2018, **2018**(4), DOI: 10.1101/pdb.prot095687.
54 F. Di Virgilio, T. H. Steinberg and S. C. Silverstein, *Methods Cell Biol.*, 1989, **31**, 453–462.
55 F. Ceriani, C. D. Ciubotaru, M. Bortolozzi and F. Mammano, *Methods Mol. Biol.*, 2016, **1427**, 223–241.
56 M. J. Levesque and R. M. Nerem, *J. Biomech. Eng.*, 1985, **107**, 341–347.
57 S. K. Bosher and R. L. Warren, *Nature*, 1978, **273**, 377–378.
58 F. Mammano and M. Bortolozzi, in *Calcium Measurement Methods*, ed. A. Verkhratsky and O. Petersen, Humana Press, New York, 2010, vol. 43, pp. 57–80.

59 I. von Kugelgen, *Pharmacol. Ther.*, 2006, **110**, 415–432.
60 R. Janssens, P. Paindavoine, M. Parmentier and J. M. Boeynaems, *Br. J. Pharmacol.*, 1999, **127**, 709–716.
61 J. B. Schachter and T. K. Harden, *Br. J. Pharmacol.*, 1997, **121**, 338–344.
62 S. Langlois, K. N. Cowan, Q. Shao, B. J. Cowan and D. W. Laird, *Mol. Biol. Cell*, 2008, **19**, 912–928.
63 W. Denk, J. H. Strickler and W. W. Webb, *Science*, 1990, **248**, 73–76.
64 S. A. Levesque, E. G. Lavoie, J. Lecka, F. Bigonnesse and J. Sevigny, *Br. J. Pharmacol.*, 2007, **152**, 141–150.
65 T. D. Westfall, C. Kennedy and P. Sneddon, *Br. J. Pharmacol.*, 1996, **117**, 867–872.
66 A. M. Kettlun, L. Uribe, V. Calvo, S. Silva, J. Rivera, M. Mancilla, M. A. Valenzuela and A. Traverso-Cori, *Phytochemistry*, 1982, **21**(3), 551–558.
67 H.-W. Yeh and H.-W. Ai, *Annu. Rev. Anal. Chem.*, 2019, **12**, 129–150.
68 I. Fasciani, A. Temperan, L. F. Perez-Atencio, A. Escudero, P. Martinez-Montero, J. Molano, J. M. Gomez-Hernandez, C. L. Paino, D. Gonzalez-Nieto and L. C. Barrio, *Neuropharmacology*, 2013, **75**, 479–490.
69 P. Whyte-Fagundes and G. Zoidl, *Biochim. Biophys. Acta, Biomembr.*, 2018, **1860**, 65–71.
70 D. Patel, X. Zhang and R. D. Veenstra, *FEBS Lett.*, 2014, **588**, 1372–1378.
71 Z. Ruan, I. J. Orozco, J. Du and W. Lü, *Nature*, 2020, DOI: 10.1038/s41586-020-2357-y.
72 J. V. Rocheleau and D. W. Piston, *Methods Cell Biol.*, 2008, **89**, 71–92.
73 L. Bousse, *Sens. Actuators, B*, 1996, **34**, 270–275.
74 J. J. Pancrazio, J. P. Whelan, D. A. Borkholder, W. Ma and D. A. Stenger, *Ann. Biomed. Eng.*, 1999, **27**, 697–711.
75 C. Giorgi, A. Danese, S. Missiroli, S. Patergnani and P. Pinton, *Trends Cell Biol.*, 2018, **28**, 258–273.
76 G. A. Ransford, N. Fregien, F. Qiu, G. Dahl, G. E. Conner and M. Salathe, *Am. J. Respir. Cell Mol. Biol.*, 2009, **41**, 525–534.
77 M. Sridharan, S. P. Adderley, E. A. Bowles, T. M. Egan, A. H. Stephenson, M. L. Ellsworth and R. S. Sprague, *Am. J. Physiol.*, 2010, **299**, H1146–H1152.
78 E. Dolmatova, G. Spagnol, D. Boassa, J. R. Baum, K. Keith, C. Ambrosi, M. I. Kontaridis, P. L. Sorgen, G. E. Sosinsky and H. S. Duffy, *Am. J. Physiol.*, 2012, **303**, H1208–H1218.
79 J. K. Sandilos, Y. H. Chiu, F. B. Chekeni, A. J. Armstrong, S. F. Walk, K. S. Ravichandran and D. A. Bayliss, *J. Biol. Chem.*, 2012, **287**, 11303–11311.
80 G. Dahl, F. Qiu and J. Wang, *Neuropharmacology*, 2013, **75**, 583–593.
81 J. M. Beckel, S. L. Daugherty, P. Tyagi, A. S. Wolf-Johnston, L. A. Birder, C. H. Mitchell and W. C. de Groat, *J. Physiol.*, 2015, **593**, 1857–1871.
82 J. M. Abitbol, J. J. Kelly, K. Barr, A. L. Schormans, D. W. Laird and B. L. Allman, *Biochem. J.*, 2016, **473**, 4665–4680.
83 J. M. Abitbol, B. L. O'Donnell, C. B. Wakefield, E. Jewlal, J. J. Kelly, K. Barr, K. E. Willmore, B. L. Allman and S. Penuela, *J. Mol. Med.*, 2019, **97**, 723–736.
84 P. Whyte-Fagundes, R. Siu, C. Brown and G. Zoidl, *Neurosci. Lett.*, 2019, **695**, 32–39.
85 F. J. Del Castillo and I. Del Castillo, *Front. Mol. Neurosci.*, 2017, **10**, 428.
86 G. Crispino, F. Galindo Ramirez, M. Campioni, V. Zorzi, M. Praetorius, G. Di Pasquale, J. A. Chiorini and F. Mammano, *Sci. Rep.*, 2017, **7**, 6567.
87 C. Clair, L. Combettes, F. Pierre, P. Sansonetti and G. Tran Van Nhieu, *Exp. Cell Res.*, 2008, **314**, 1250–1265.
88 E. G. Harks, A. D. de Roos, P. H. Peters, L. H. de Haan, A. Brouwer, D. L. Ypey, E. J. van Zoelen and A. P. Theuvenet, *J. Pharmacol. Exp. Ther.*, 2001, **298**, 1033–1041.
89 R. Guinamard, C. Simard and C. Del Negro, *Pharmacol. Ther.*, 2013, **138**, 272–284.
90 K. Michalski and T. Kawate, *J. Gen. Physiol.*, 2016, **147**, 165–174.
91 A. W. Lohman and B. E. Isakson, *FEBS Lett.*, 2014, **588**, 1379–1388.
92 Y. Kuang, V. Zorzi, D. Buratto, G. Ziraldo, F. Mazzarda, C. Peres, C. Nardin, A. M. Salvatore, F. Chiani, F. Scavizzi, M. Raspa, M. Qiang, Y. Chu, X. Shi, Y. Li, L. Liu, Y. Shi, F. Zonta, G. Yang, R. A. Lerner and F. Mammano, *EBioMedicine*, 2020, 102825, DOI: 10.1016/j.ebiom.2020.102825.
93 Z. Wu and Y. Li, *Neurosci. Res.*, 2020, **152**, 35–43.